Research Article

Utilizing the full capacity of carbon black as anode for Na-ion batteries via solvent co-intercalation

Wei Xiao[1,2], Qian Sun[1], Jian Liu[1], Biwei Xiao[1], Per-Anders Glans[3], Jun Li[2], Ruying Li[1], Jinghua Guo[3], Wanli Yang[3], Tsun-Kong Sham[2] (✉), and Xueliang Sun[1] (✉)

[1] Department of Mechanical & Materials Engineering, University of Western Ontario, London, Ontario N6A5B9, Canada
[2] Department of Chemistry, University of Western Ontario, London, Ontario N6A5B7, Canada
[3] Advanced Light Source, Lawrence Berkeley National Laboratory, Berkeley, California 94720, USA

ABSTRACT

Carbonaceous materials have long been considered promising anode materials for Na-ion batteries. However, the electrochemical performance of conventional carbon anodes is generally poor because the sodium ion storage solely relies on the disordered region of the carbon materials in a carbonate-based electrolyte. The solvent co-intercalation mechanism for Na ions has been recently reported in natural graphite anodes for Na-ion batteries with ether-based electrolytes, but their capacities are still unsatisfactory. We show here for the first time that by combining regular Na ion storage in the disordered carbon layer and solvent co-intercalation mechanism in the graphitized layer of a commercial N330 carbon black as an anode material for Na-ion batteries in ether-based electrolyte, the reversible capacity could be fully realized and doubled in magnitude. This unique sodium intercalation process resulted in a significantly improved electrochemical performance for the N330 electrode with an initial reversible capacity of 234 mAh·g^{-1} at 50 mA·g^{-1} and a superior rate capability of 105 mAh·g^{-1} at 3,200 mA·g^{-1}. When cycled at 3,200 mA·g^{-1} over 2,000 cycles, the electrode still exhibited a highly reversible capacity of 72 mAh·g^{-1} with a negligible capacity loss per cycle (0.0167%). Additionally, surface-sensitive C K-edge X-ray absorption spectroscopy, with the assistance of electrochemical and physicochemical characterizations, helped in identifying the controlled formation and evolution of a thin and robust solid electrolyte interphase film. This film not only reduced the resistance for sodium ion diffusion, but also maintained the structural stability of the electrode for extended cycle reversibility. The superior electrochemical performance of N330 carbon black strongly demonstrated the potential of applying ether-based electrolytes for a wide range of carbon anodes apart from natural graphite.

Address correspondence to Xueliang Sun, xsun9@uwo.ca; Tsun-Kong Sham, tsham@uwo.ca

TSINGHUA UNIVERSITY PRESS Springer

1   Introduction

Since the successful commercialization of lithium-ion batteries (LIBs) in the portable electronics market, the geological concentration of lithium sources, along with the soaring price of Li in recent years, led to the development of sustainable and affordable energy storage systems [1, 2]. Sodium-ion batteries (SIBs), which benefit from the natural abundance of sodium and similar electrochemical reaction mechanism to lithium counterparts, have been frequently revisited and suggested as competitive alternatives for LIBs, especially in applications of large-scale grid energy storage [3–5]. However, shifting the charge carriers from the lithium ions to sodium ions would inevitably trigger kinetics issues relating to the larger ionic radius of Na$^+$ (1.02 Å), and the energy density disadvantages regarding the higher redox potential (−2.71 V vs. SHE) as well as the larger atomic weight [6]. The relatively low desolvation energy for the Na ion and comparatively small activation energy for Na ion diffusion may envision the great potential for high-performance SIBs [7, 8].

Considering the safety issues surrounding the direct use of metallic sodium as an anode, such as its low melting point (97.7 ℃) and dendritic growth, carbonaceous materials have been considered promising alternatives. However, due to the difficulty of sodium intercalation into graphite for energetically unstable Na-graphite intercalated compounds [9–12], hard carbon with a large interlayer spacing in a disordered structure was applied as a high-capacity anode material [13, 14]. In the last decade, a great deal of effort has been devoted to rationally designing the structure of insertion-type anode materials [15–17] and developing a high-performance composite anode based on multi-electron alloy/conversion reactions for more efficient sodium storage [18, 19]. Furthermore, optimization of the electrolyte seems to be feasible for controlling the solid electrolyte interphase (SEI) formation and ameliorating the electrochemical performance [20, 21]. Adelhelm et al. [22] reported the first application of graphite in a diglyme-based electrolyte, demonstrating a significant increase in capacity as compared to cells using traditional carbonate-based electrolytes. This additional Na ion storage was resulted from the co-intercalation of solvent molecules into the graphite layers. Kang et al. [23, 24] further studied the electrochemical reactions of natural graphite in different ether-based electrolytes, while the concept of solvent co-intercalation was applied for sodium ion storage in graphite [25–32]. These works have proved that solvated sodium ion compounds can reversibly intercalate into layered structures via the formation of ternary graphite intercalation compounds (t-GICs). These studies indicate a new strategy for the use of ordered graphite as the anode for SIBs. However, the reported natural graphite anodes exhibit a low capacity (below 150 mAh·g^{-1}) even at low current rates below 100 mA·g^{-1}. Thus, it is worthy to know whether this strategy will improve the electrochemical performance of common carbon materials with both disordered and graphitic structures.

In this work, a commercial carbon black material is chosen and examined for use in SIBs with an ether-based electrolyte, to gauge the feasibility of employing both disordered and graphitic structures in sodium ion storage for an improved electrochemical performance. Surprisingly, a highly reversible capacity with an extended cycle life is obtained, and a reaction mechanism combining sodium intercalation in the graphitic structure with that in the disordered structure for ether-based electrolytes is proposed.

2   Experimental

2.1   Materials preparation

Commercial N330 carbon black (Sid Richardson Carbon Corporation) was selected as the active material. Two electrolytes were prepared in an argon-filled glove box from 1.0 M sodium triflate (NaCF$_3$SO$_3$, 98%, Sigma Aldrich) dissolved in two different solvents, diethylene glycol dimethyl ether (DEGDME, 98.9%, Sigma-Aldrich) and ethylene carbonate (EC, 99%, BASF)/diethyl carbonate (DEC, 99%, BASF) with 1:1 in volume ratio. Before preparing the electrolytes, NaCF$_3$SO$_3$ and molecular sieves (4 Å, Sigma Aldrich) were dried at 150 ℃ in a vacuum oven for 2 days, while molecular sieves were later employed to dehydrate the solvent.

2.2 Characterizations

The physical properties of the pristine material were identified by an X-ray diffraction (XRD) Bruker D8Advance (Cu-Kα source, 40 kV, 40 mA) system. Raman scattering studies were performed using a HORIBA Scientific LabRAM HR Raman spectrometer system with a 532.4 nm laser and optical microscope. Fourier transform infrared (FTIR) spectra were collected using a Nicolet 6700 FTIR spectrometer. N_2 adsorption/ desorption isotherms were collected using a Folio Micromeritics Tristar II surface area analyzer, while morphology was observed with a Hitachi S-4800 field emission scanning electron microscope (FE-SEM) operating at 5 keV. In order to gain an understanding of the underlying reaction mechanism, the cycled electrodes at different electrochemical states were extracted from the cells and further characterized by X-ray diffraction (XRD), Raman scattering spectra, and C K-edge X-ray absorption spectroscopy (XAS). XAS experiments were conducted in Beamline 6.3.1 of the Advanced Light Source (ALS) in Lawrence Berkley National Laboratory. The C 1s X-ray photoemission spectroscopy (XPS) experiments were carried out at the high resolution Spherical Grating Monochromator (SGM) beamline in the Canadian Light Source (CLS).

To fabricate the N330 carbon electrode, a slurry was initially prepared by mixing 80 wt.% active material, 10 wt.% acetylene black as conductive agent, and 10 wt.% poly(vinylidene difluoride) (PVDF) binder with N-methyl pyrrolidinone and doctor bladed onto a copper foil. After drying at 80 °C under vacuum for 12 h, the electrode was punched and pressed into 1/2-inch pellets, which were further pressed with a loading mass of about 0.8 mg·cm^{-2}. CR-2032 coin cells were assembled using sodium foil as an anode, N330 carbon electrode as a cathode, and a polypropylene micro-porous film (Celgard 2400) as a separator, in a glove box under argon atmosphere with controlled moisture and oxygen content.

Cyclic voltammetry (CV) experiments were performed using a potentiated 3/Z (Biologic VMP3) system at 0.1 mV·s^{-1}, while electrochemical impedance spectra (EIS) were recorded at an alternating current (AC) voltage of 5 mV amplitude in the 100 kHz to 0.01 Hz frequency range. The galvanostatic charge/discharge performances were characterized between 0.001–2.5 V (vs. Na/Na$^+$) for different current densities at room temperature, using an Arbin BT-2000 Battery Tester.

3 Results and discussion

The coexistence of disordered and graphitic carbon in N330 carbon black was first identified by XRD (Fig. S1(a) in the Electronic Supplementary Material (ESM)) and Raman spectroscopy (Fig. S1(b) in the ESM), which structurally display graphitic characteristics with a larger interlayer spacing and disordered feature with defects. The existence of several functional groups was also confirmed from the results of FTIR (Fig. S1(c) in the ESM) and synchrotron-based XPS (Fig. S1(d) in the ESM).

The electrochemical performance of N330 carbon black as an electrode in SIBs with the ether (DEGDME)- and carbonate (EC/DEC)-based electrolytes was evaluated by discharging and charging in 2032 coin cells along with Na foil as a counter electrode between 0.001 and 2.5 V (vs. Na/Na$^+$) at different current densities. Figures 1(a) and 1(b) show the discharge/charge profiles of N330 carbon black electrode in different electrolytes at a current density of 50 mA·g^{-1}. The electrode cycled in the DEGDME-based electrolyte delivers an initial reversible capacity of 234 mAh·g^{-1} with a Coulombic efficiency of 61.45%. This value is double that of the initial reversible capacity of 107 mAh·g^{-1} and Coulombic efficiency of 39.05% obtained with the EC/DEC-based electrolyte. Although the reversible capacity of the electrodes gradually decreased for both the electrolyte systems, the cell constructed using a DEGDME-based electrolyte maintains higher charging capacities of 230, 226, 212, 207, 202, and 196 mAh·g^{-1} at the 2nd, 3rd, and 100th cycles, respectively; the electrode cycled in EC/ DEC-based electrolyte presents reversible capacities of just 103, 101, 90, 86, 82, and 79 mAh·g^{-1}, respectively, at the 2nd, 3rd, and 100th cycles. Figure 1(c) further compares the cycle stability of the N330 carbon black electrode in different electrolytes. After 100 cycles, the electrode prepared in DEGDME electrolyte demonstrates a capacity retention of 85.2%, while the electrode cycled in EC/DEC shows a capacity retention
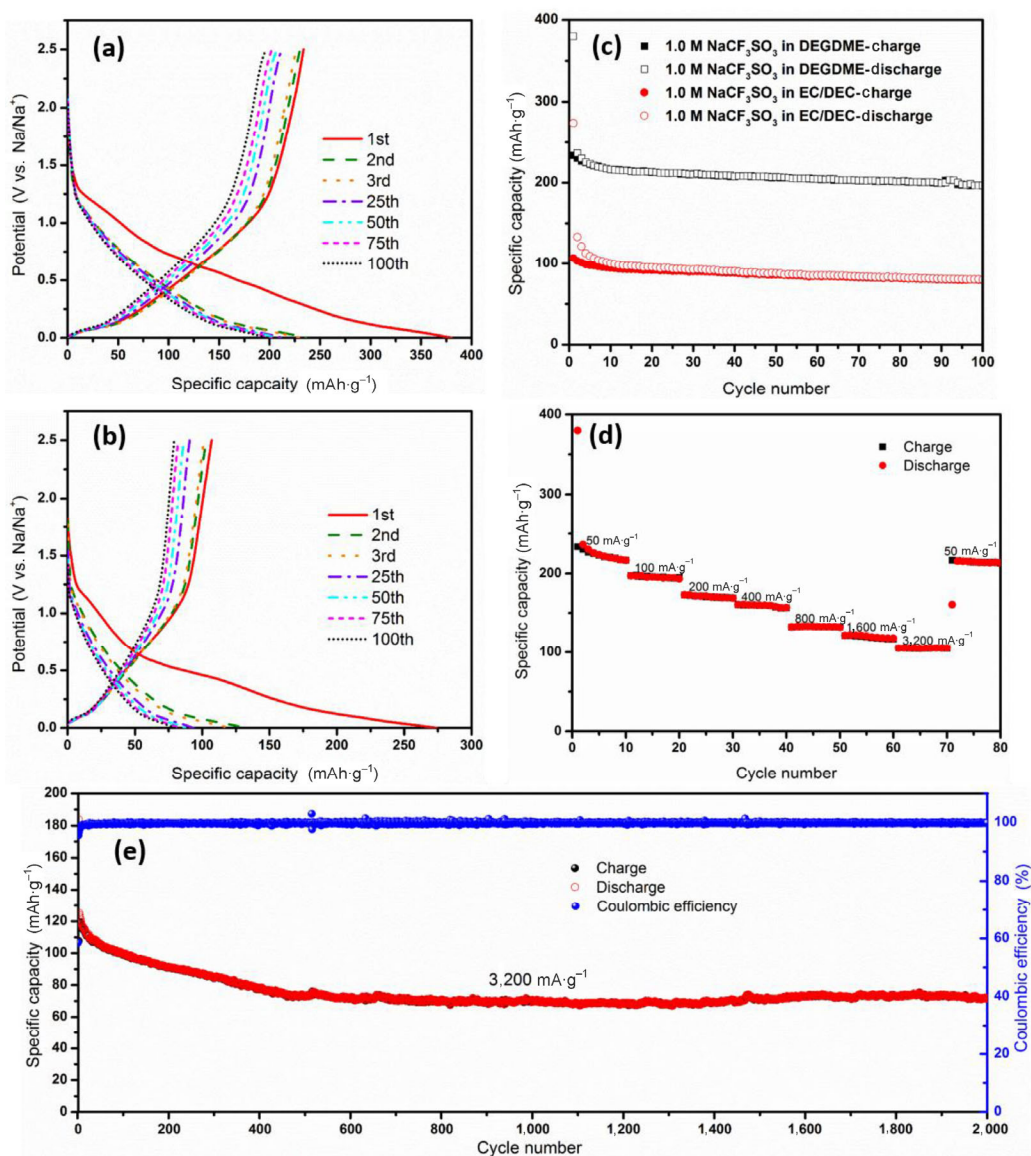
Figure 1 Discharge/charge profiles of the N330 carbon black electrode in electrolyte using (a) DEGDME and (b) EC/DEC (1:1) as solvents, at a current density of 50 mA·g^{-1}. (c) Cycle performances of N330 carbon black in different electrolytes at a current density of 50 mA·g^{-1}. (d) Rate performance at various current densities and (e) rate cycle performance at 3,200 mA·g^{-1} for N330 carbon black in electrolyte using DEGDME as solvent.

of 76.7%. Furthermore, a stable cycle life can be obtained in the ether-based electrolyte at 100 and 200 mA·g^{-1}, as shown in Fig. S6 in the ESM.

When cycled at 100, 200, 400, 800, 1,600, and 3,200 mA·g^{-1}, the N330 carbon black electrode maintains reversible capacities of 196, 170, 159, 133, 120, and 105 mAh·g^{-1}, respectively. Even when the cell is cycled at 3,200 mA·g^{-1} for 2,000 cycles, a highly reversible capacity of 72 mAh·g^{-1} is obtained, representing a negligible capacity loss per cycle of 0.0167%

(Fig. 1(e)). Compared with previous results obtained from expanded graphite [33] and graphite [22–25, 27, 29–32], the sodium storage capability and cyclability for N330 carbon black in DEGDME-based electrolyte are greatly improved. Crucially, the feasibility of a sodium-ion battery exploiting N330 carbon black as an anode material has been confirmed in conjunction with a Na$_{0.7}$CoO$_2$ cathode material in an ether-based electrolyte, regardless of its relatively low capacity and limited cycle capability (Fig. S7 in the ESM).

To obtain an in-depth understanding of the improved sodium storage behavior observed for the N330 carbon black electrodes, various characterization tools were employed. Figure 2(a) compares the initial CV curves for carbon black cycled in different solvents. Interestingly, the cathodic peak at 0.5 V observed for the carbonate-based electrolyte is not found in the CV obtained for the electrode cycled in the DEGDME-based electrolyte. This indicates a controlled formation of the SEI [23]. Previous literature mentions that an electronically insulating thin SEI film may effectively suppress the continuous decomposition of electrolyte at low potential and stabilize the layered structure of graphitic carbon for an extended cycle life, in case of its fragility towards solvent co-intercalation for LIBs [34, 35]. At the same time, comparison of EIS for the N330 carbon black electrodes (Fig. 2(b)) before and after discharging in different electrolytes also confirms the importance of appropriate SEI formation for the electrode sodiation/desodiation process. For the discharged anodic electrodes, it is assumed that the value of the horizontal axis intercept is related to the SEI impedance between electrode and electrolyte in the high frequency region. The semicircle in the medium frequency region could be attributed to charge transfer resistance, while the linear region corresponds to the Warburg resistance for Na$^+$ diffusion in the bulk [36]. When EC/DEC was applied as solvent in the electrolyte, the comparatively thick SEI layer formed in the initial discharging process (Fig. S4 in the ESM) results in an increase of resistance for sodium ion diffusion, while a negligibly thin SEI film is formed on the surface of electrodes cycled in DEGDME-based electrolyte, resulting in the facile migrations of sodium ions and solvated compounds, thereby enhancing the electrochemical sodiation/desodiation processes. A comparison of the impedance parameters for electrodes at different states in different electrolytes can be found in Table S1 in the ESM. Raman spectra (Fig. 2(c)) were employed to identify the structural evolution of N330 carbon black in the DEGDME-based electrolyte during the sodiation/desodiation process. The ratio of I_D/I_G decreases remarkably when the cells are discharged to 0.001 V. However, subsequent charging to 2.5 V results in reversibility, hinting a better alignment between the carbon layers during the sodiation

process. Similar results, i.e. the decrease of I_D/I_G in the discharging process and its successive increase in the charging process, were obtained in *ex situ* Raman spectra (Fig. S8 and Table S2 in the ESM). The positions and shapes of the D/G bands did not change upon cycling, although their intensities continue to decrease. Although this phenomenon is similar to the phase transformations seen in partially ordered carbon in EC/DEC-based electrolyte [37], it is quite different with regard to the formation of disordered structures [23], further implying the complexity of electrochemical behaviors and phase transformations for different carbon materials in ether-based electrolytes. Figure 2(d) displays the C K-edge X-ray absorption spectroscopies obtained in the TEY mode, which is exceptionally sensitive to the physicochemical properties of the surface. For the pristine electrode, two broad peaks involving the transitions of carbon 1s electrons to unoccupied π^*(C–C) and σ^*(C–C) [38] can be observed at 285.3 and 292.2 eV, respectively, while the weak feature near 288.2 eV is assigned to the C=O π^* transition [38–41]. After discharging to 0.01 V, the positions of the π^*(C–C) and π^*(C=O) features move to the high energy region, while the peak for the σ^*(C–C) transition disappears. Simultaneously, the peak intensity for π^*(C=O) obviously increases and a new sharp peak appears at 290.0 eV, originating from σ^*(C–O) transitions for oxygen-containing functional groups [41–43], further indicating the decomposition of electrolyte and formation of SEI on the surface of the electrode during the sodiation process. The broad peak around 301.0 eV may be related to the σ^*(C=O) feature [42–44]. When charged back to 2.5 V, the π^*(C–C) feature and weak σ^*(C–C) feature both move back to their initial positions at pristine state, while the electrode still presents the visible features for π^*(C=O) and σ^*(C–O) transitions, confirming the preservation of a thin SEI film for the N330 carbon black electrode, which is beneficial to the structural stability in the long run [28]. Although CV curves cannot reflect the formation of the SEI during the initial cathodic process for the N330 carbon black electrode, the C K-edge X-ray absorption spectroscopic technique could explicitly identify the decomposition of electrolyte upon discharging and the evolution of a thin SEI layer during the sodiation/desodiation process, which agrees
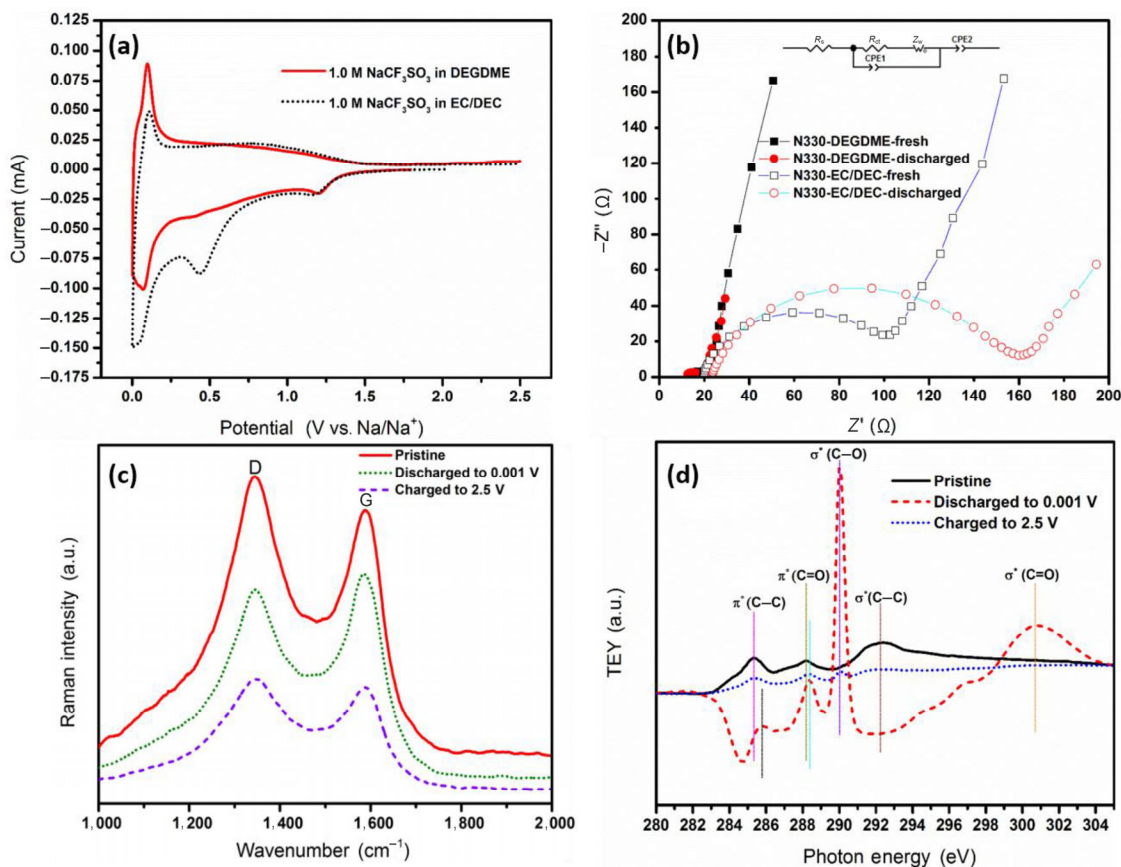
Figure 2 (a) The CV curves of the first cycle for N330 carbon black electrodes in different electrolytes. (b) EIS for N330 carbon black electrodes before and after discharging in different electrolytes (the inset shows the equivalent circuit model). (c) Raman spectra and (d) C K-edge X-ray absorption spectroscopies of N330 carbon black electrodes at different states when cycling in DEGDME-based electrolyte.

well with the reduced resistance and increased capacity as discussed in the electrochemical properties of N330 carbon black electrode in DEGDME-based electrolyte. Importantly, the ether-based electrolyte is supposed to suppress the decomposition of electrolyte and generate a thin SEI layer.

This robust and uniform SEI layer could inhibit depletion of the electrolyte in irreversible side reactions between the electrode surface and electrolyte, and further facilitate the rapid Na+ transport with assistance of the uniform distribution of organic and inorganic compounds [28]. Similar functions of the ether-based electrolyte could be observed in formation of a compact and thin SEI layer on surface of sodium metal to prevent the exposure of the active sodium metal surface to the electrolyte and avoid the growth of sodium dendrite during the long-term plating and stripping [45]. In terms of morphological evolution,

the N330 carbon black electrode could maintain its nanostructures in ether-based electrolyte during the discharging and charging processes, but undergo aggregation upon cycling in carbonate-based electrolyte, as shown in Fig. S10 in the ESM.

According to the classic "house of cards" model [13, 46] and its recent revision [47] for sodium storage mechanism in nongraphitizable carbon, the graphene sheets with a larger interlayer distance and massive defects as well as nanoporosity in disordered turbostratic nanodomains will contribute to the sodium intercalation process. However, this cannot explain the significant increase in capacity observed for N330 carbon black in ether-based electrolyte compared to carbonate-based electrolyte. As revealed by Adelhelm et al. [22] and Kang et al. [23, 24], the solvated sodium ion species in ether-based electrolyte may effectively facilitate sodium intercalation into graphitic carbon.
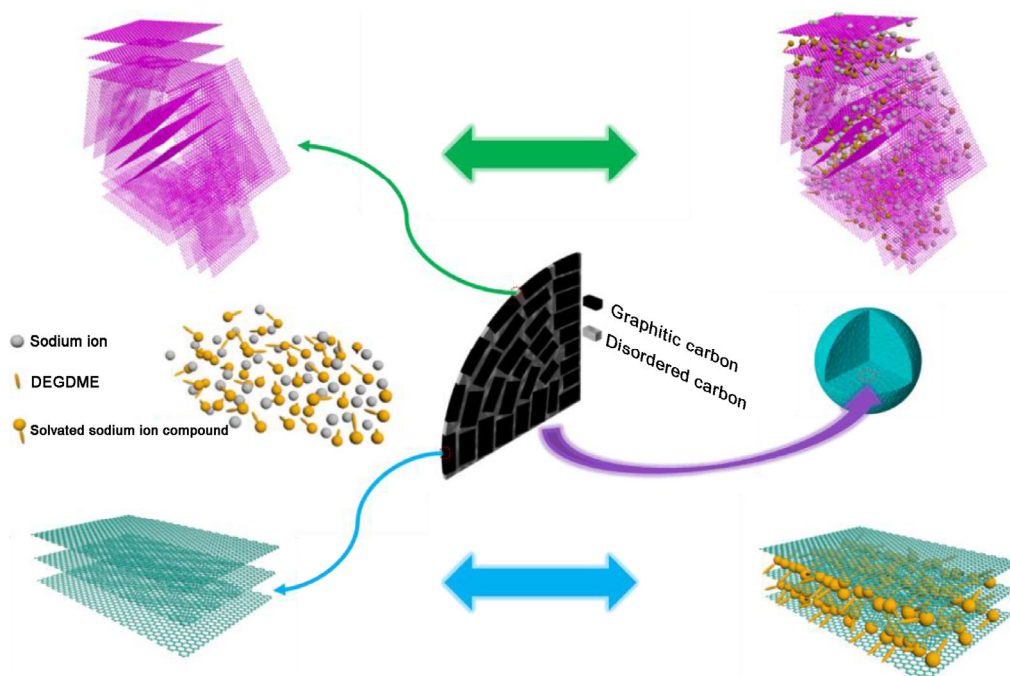
Figure 3 Schematic diagram of sodium intercalation in N330 carbon black.

Later, Zhen Zhou et al. [26] reported the improved cycle stability and rate capability for hard carbon material with a disordered structure in ether-based electrolyte.

Based on these sodium storage mechanisms in disordered and graphitic carbon structures as well as a greatly enhanced electrochemical performance in N330 carbon black consisting of graphitic structure and disordered structure [26, 28, 48, 49], a sodium storage mechanism combining the sodium ion insertion into disordered carbon with sodium ion-solvent co-intercalation into graphitic carbon can be accordingly proposed here (Fig. 3). The sodium ions and solvated sodium ion species would preferably intercalate into different structural parts of the N330 carbon black, even though the preference for different sodium intercalation mechanisms in disordered carbon is still unknown. Specifically, most solvated sodium ion species would intercalate into graphitic structures, while partially solvated sodium ion species and residual sodium ions could insert into disordered structures. By making most of the accessible sodium storage sites in both the graphitic and disordered parts of N330 carbon black, the reversible capacity and cycle stability could be promoted in the DEGDME-based

electrolyte, compared with limited sodium intercalation capability and stability in EC/DEC-based electrolyte.

In summary, the improved electrochemical properties for N330 carbon black in ether-based electrolyte are not only resulted from novel intercalation mechanisms, but also due to the controlled formation of a robust and thin SEI film coating the electrode. The advantages of using an ether-based electrolyte rekindle the interests in insertion-type anode materials using ether-based electrolyte, and the development of high performance carbon anode materials in ether-based electrolytes for sodium ion batteries is ongoing in our group.

4   Conclusion

The combination of sodium ion storage in disordered carbon layers and solvated sodium ion compounds co-intercalation into graphitic carbon layers for a commercial N330 carbon black electrode resulted in a very high electrochemical performance in an ether-based electrolyte, with a high initial reversible capacity of 234 mAh·g^{-1} and a significantly enhanced rate capability of 105 mAh·g^{-1} at 3,200 mAh·g^{-1}, as

well as an ultralong cycle life over 2,000 cycles. Additionally, the restricted formation of the SEI film and its subsequent evolution as clarified by electrochemical and physical characterizations would also contribute to the superior electrochemical performance for ether-based electrolyte, especially when compared with the poor sodium storage capability and uncontrollable formation of a thick SEI layer for carbonate-based electrolyte. The application of advantageous ether-based electrolytes in carbon-based materials could shed light on the design of advanced SIBs with the higher reversible capacity and better cycle stability.

Acknowledgements

Electronic Supplementary Material: Supplementary material (physicochemical properties, morphologies and electrochemical properties for N330 carbon black) is available in the online version of this article at https://doi.org/10.1007/s12274-017-1852-4.

References

[1] Tarascon, J. M. Is lithium the new gold? *Nat. Chem.* **2010**, *2*, 510.

[2] Kundu, D.; Talaie, E.; Duffort, V.; Nazar, L. F. The emerging chemistry of sodium ion batteries for electrochemical energy storage. *Angew. Chem., Int. Ed.* **2015**, *54*, 3431–3448.

[3] Yabuuchi, N.; Kubota, K.; Dahbi, M.; Komaba, S. Research development on sodium-ion batteries. *Chem. Rev.* **2014**, *114*, 11636–11682.

[4] Palomares, V.; Serras, P.; Villaluenga, I.; Hueso, K. B.; Carretero-González, J.; Rojo, T. Na-ion batteries, recent advances and present challenges to become low cost energy storage systems. *Energy Environ. Sci.* **2012**, *5*, 5884–5901.

[5] Pan, H. L.; Hu, Y.-S.; Chen, L. Q. Room-temperature stationary sodium-ion batteries for large-scale electric energy storage. *Energy Environ. Sci.* **2013**, *6*, 2338–2360.

[6] Hong, S. Y.; Kim, Y.; Park, Y.; Choi, A.; Choi, N.-S.; Lee, K. T. Charge carriers in rechargeable batteries: Na ions vs. Li ions. *Energy Environ. Sci.* **2013**, *6*, 2067–2081.

[7] Okoshi, M.; Yamada, Y.; Yamada, A.; Nakai, H. Theoretical analysis on de-solvation of lithium, sodium, and magnesium cations to organic electrolyte solvents. *J. Electrochem. Soc.* **2013**, *160*, A2160–A2165.

[8] Ong, S. P.; Chevrier, V. L.; Hautier, G.; Jain, A.; Moore, C.; Kim, S.; Ma, X. H.; Ceder, G. Voltage, stability and diffusion barrier differences between sodium-ion and lithium-ion intercalation materials. *Energy Environ. Sci.* **2011**, *4*, 3680–3688.

[9] Asher, R. C. A lamellar compound of sodium and graphite. *J. Inorg. Nucl. Chem.* **1959**, *10*, 238–249.

[10] DiVincenzo, D. P.; Mele, E. J. Self-consistent effective-mass theory for intralayer screening in graphite intercalation compounds. *Phys. Rev. B* **1984**, *29*, 1685–1694.

[11] Ge, P.; Fouletier, M. Electrochemical intercalation of sodium in graphite. *Solid State Ionics* **1988**, *28–30*, 1172–1175.

[12] Nobuhara, K.; Nakayama, H.; Nose, M.; Nakanishi, S.; Iba, H. First-principles study of alkali metal-graphite intercalation compounds. *J. Power Sources* **2013**, *243*, 585–587.

[13] Stevens, D. A.; Dahn, J. R. High capacity anode materials for rechargeable sodium-ion batteries. *J. Electrochem. Soc.* **2000**, *147*, 1271–1273.

[14] Doeff, M. M.; Ma, Y. P.; Visco, S. J.; De Jonghe, L. C. Electrochemical insertion of sodium into carbon. *J. Electrochem. Soc.* **1993**, *140*, L169–L170.

[15] Xie, X. Q.; Ao, Z. M.; Su, D. W.; Zhang, J. Q.; Wang, G. X. MoS$_2$/graphene composite anodes with enhanced performance for sodium-ion batteries: The role of the two-dimensional heterointerface. *Adv. Funct. Mater.* **2015**, *25*, 1393–1403.

[16] Xie, X. Q.; Zhao, M.-Q.; Anasori, B.; Maleski, K.; Ren, C. E.; Li, J. W.; Byles, B. W.; Pomerantseva, E.; Wang, G.; Gogotsi, Y. Porous heterostructured MXene/carbon nanotube composite paper with high volumetric capacity for sodium-based energy storage devices. *Nano Energy* **2016**, *26*, 513–523.

[17] Xie, X. Q.; Makaryan, T.; Zhao, M. Q.; Van Aken, K. L.; Gogotsi, Y.; Wang, G. X. MoS$_2$ nanosheets vertically aligned on carbon paper: A freestanding electrode for highly reversible sodium-ion batteries. *Adv. Energy Mater.* **2016**, *6*, 1502161.

[18] Bommier, C.; Ji, X. L. Recent development on anodes for Na-ion batteries. *Isr. J. Chem.* **2015**, *55*, 486–507.

[19] Kim, Y.; Ha, K. H.; Oh, S. M.; Lee, K. T. High-capacity anode materials for sodium-ion batteries. *Chem.—Eur. J.* **2014**, *20*, 11980–11992.

[20] Ponrouch, A.; Dedryvère, R.; Monti, D.; Demet, A. E.; Ateba Mba, J. M.; Croguennec, L.; Masquelier, C.; Johansson, P.; Palacín, M. R. Towards high energy density sodium ion batteries through electrolyte optimization. *Energy Environ. Sci.* **2013**, *6*, 2361–2369.

[21] Ponrouch, A.; Marchante, E.; Courty, M.; Tarascon, J.-M.; Palacín, M. R. In search of an optimized electrolyte for Na-ion batteries. *Energy Environ. Sci.* **2012**, *5*, 8572–8583.

[22] Jache, B.; Adelhelm, P. Use of graphite as a highly reversible electrode with superior cycle life for sodium-ion batteries by making use of Co-intercalation phenomena. *Angew. Chem., Int. Ed.* **2014**, *53*, 10169–10173.

[23] Kim, H.; Hong, J.; Park, Y.-U.; Kim, J.; Hwang, I.; Kang, K. Sodium storage behavior in natural graphite using ether-based electrolyte systems. *Adv. Funct. Mater.* **2015**, *25*, 534–541.

[24] Kim, H.; Hong, J.; Yoon, G.; Kim, H.; Park, K.-Y.; Park, M.-S.; Yoon, W.-S.; Kang, K. Sodium intercalation chemistry in graphite. *Energy Environ. Sci.* **2015**, *8*, 2963–2969.

[25] Jung, S. C.; Kang, Y.-J.; Han, Y.-K. Origin of excellent rate and cycle performance of Na$^+$-solvent cointercalated graphite vs. poor performance of Li$^+$-solvent case. *Nano Energy* **2017**, *34*, 456–462.

[26] Zhu, Y.-E.; Yang, L. P.; Zhou, X. L.; Li, F.; Wei, J. P.; Zhou, Z. Boosting the rate capability of hard carbon with an ether-based electrolyte for sodium ion batteries. *J. Mater. Chem. A* **2017**, *5*, 9528–9532.

[27] Seidl, L.; Bucher, N.; Chu, E.; Hartung, S.; Martens, S.; Schneider, O.; Stimming, U. Intercalation of solvated Na-ions into graphite. *Energy Environ. Sci.* **2017**, *10*, 1631–1642.

[28] Zhang, J.; Wang, D.-W.; Lv, W.; Zhang, S. W.; Liang, Q. H.; Zheng, D. Q.; Kang, F. Y.; Yang, Q.-H. Achieving superb sodium storage performance on carbon anodes through an ether-derived solid electrolyte interphase. *Energy Environ. Sci.* **2017**, *10*, 370–376.

[29] Jache, B.; Binder, J. O.; Abe, T.; Adelhelm, P. A comparative study on the impact of different glymes and their derivatives as electrolyte solvents for graphite co-intercalation electrodes in lithium-ion and sodium-ion batteries. *Phys. Chem. Chem. Phys.* **2016**, *18*, 14299–14316.

[30] Guan, Z. X.; Shen, X.; Yu, R. C.; Wang, Z. X.; Chen, L. Q. Chemical intercalation of solvated sodium ions in graphite. *Electrochim. Acta* **2016**, *222*, 1365–1370.

[31] Hasa, I.; Dou, X. W.; Buchholz, D.; Shao-Horn, Y.; Hassoun, J.; Passerini, S.; Scrosati, B. A sodium-ion battery exploiting layered oxide cathode, graphite anode and glyme-based electrolyte. *J. Power Sources* **2016**, *310*, 26–31.

[32] Zhu, Z. Q.; Cheng, F. Y.; Hu, Z.; Niu, Z. Q.; Chen, J. Highly stable and ultrafast electrode reaction of graphite for

sodium ion batteries. *J. Power Sources* **2015**, *293*, 626–634.

[33] Wen, Y.; He, K.; Zhu, Y. J.; Han, F. D.; Xu, Y. H.; Matsuda, I.; Ishii, Y.; Cumings, J.; Wang, C. S. Expanded graphite as superior anode for sodium-ion batteries. *Nat. Commun.* **2014**, *5*, 4033.

[34] Peled, E. The electrochemical behavior of alkali and alkaline earth metals in nonaqueous battery systems-the solid electrolyte interphase model. *J. Electrochem. Soc.* **1979**, *126*, 2047–2051.

[35] Xu, K. Electrolytes and interphases in Li-ion batteries and beyond. *Chem. Rev.* **2014**, *114*, 11503–11618.

[36] Xiao, L. F.; Cao, Y. L.; Henderson, W. A.; Sushko, M. L.; Shao, Y. Y.; Xiao, J.; Wang, W.; Engelhard, M. H.; Nie, Z. M.; Liu, J. Hard carbon nanoparticles as high-capacity, high-stability anodic materials for Na-ion batteries. *Nano Energy* **2016**, *19*, 279–288.

[37] Lotfabad, E. M.; Kalisvaart, P.; Kohandehghan, A.; Karpuzov, D.; Mitlin, D. Origin of non-SEI related coulombic efficiency loss in carbons tested against Na and Li. *J. Mater. Chem. A* **2014**, *2*, 19685–19695.

[38] Zhou, J. G.; Zhou, X. T.; Li, R. Y.; Sun, X. L.; Ding, Z. F.; Cutler, J.; Sham, T.-K. Electronic structure and luminescence center of blue luminescent carbon nanocrystals. *Chem. Phys. Lett.* **2009**, *474*, 320–324.

[39] Zhou, J. G.; Zhou, X. T.; Sun, X. H.; Li, R. Y.; Murphy, M.; Ding, Z. F.; Sun, X. L.; Sham, T.-K. Interaction between Pt nanoparticles and carbon nanotubes—An X-ray absorption near edge structures (XANES) study. *Chem. Phys. Lett.* **2007**, *437*, 229–232.

[40] Bouchet-Fabre, B.; Pinault, M.; Pichot, V.; Launois, P.; Mayne-L'Hermite, M.; Parent, P.; Laffon, K.; Durand, D.; Reynaud, C. NEXAFS and X-ray scattering study of structure changes after post-annealing treatments of aligned MWNTs. *Diamond Relat. Mater.* **2005**, *14*, 881–886.

[41] Roy, S. S.; Papakonstantinou, P.; Okpalugo, T. I. T.; Murphy, H. Temperature dependent evolution of the local electronic structure of atmospheric plasma treated carbon nanotubes: Near edge X-ray absorption fine structure study. *J. Appl. Phys.* **2006**, *100*, 053703.

[42] Banerjee, S.; Hemraj-Benny, T.; Balasubramanian, M.; Fischer, D. A.; Misewich, J. A.; Wong, S. S. Ozonized single-walled carbon nanotubes investigated using NEXAFS spectroscopy. *Chem. Commun.* **2004**, 772–773.

[43] Kuznetsova, A.; Popova, I.; Yates Jr, J. T.; Bronikowski, M. J.; Huffman, C. B.; Liu, J.; Smalley, R. E.; Hwu, H. H.; Chen, J. G. Oxygen-containing functional groups on single-wall carbon nanotubes: NEXAFS and vibrational spectroscopic studies. *J. Am. Chem. Soc.* **2001**, *123*, 10699–10704.

[44] Nyberg, M.; Hasselström, J.; Karis, O.; Wassdahl, N.; Weinelt, M.; Nilsson, A.; Pettersson, L. G. M. The electronic structure and surface chemistry of glycine adsorbed on Cu(110). *J. Chem. Phys.* **2000**, *112*, 5420–5427.

[45] Seh, Z. W.; Sun, J.; Sun, Y. M.; Cui, Y. A highly reversible room-temperature sodium metal anode. *ACS Cent. Sci.* **2015**, *1*, 449–455.

[46] Stevens, D. A.; Dahn, J. R. The mechanisms of lithium and sodium insertion in carbon materials. *J. Electrochem. Soc.* **2001**, *148*, A803–A811.

[47] Bommier, C.; Surta, T. W.; Dolgos, M.; Ji, X. L. New mechanistic insights on Na-ion storage in nongraphitizable carbon. *Nano Lett.* **2015**, *15*, 5888–5892.

[48] Jaouen, F.; Dodelet, J.-P. Non-noble electrocatalysts for O_2 reduction: How does heat treatment affect their activity and structure? Part I. Model for carbon black gasification by NH_3: Parametric calibration and electrochemical validation. *J. Phys. Chem. C* **2007**, *111*, 5963–5970.

[49] Li, Y. L.; Li, X. F.; Geng, D. S.; Tang, Y. J.; Li, R. Y.; Dodelet, J.-P.; Lefèvre, M.; Sun, X. L. Carbon black cathodes for lithium oxygen batteries: Influence of porosity and heteroatom-doping. *Carbon* **2013**, *64*, 170–177.